molds. This technology has been previously used for the development of cardiovascular tissues with vascular grafts, namely Biotubes.[13,15] The Biotubes were formed within a relatively short period (4 weeks) after embedding rod-like molds into subcutaneous pouches because the whole mold surfaces were attached directly to the subcutaneous tissue. In comparison, since tissue migration into a small aperture is slow, leaflet formation in the Biovalves took longer, following the formation of the conduit. Therefore, in this study, non-invasive ECs were impregnated into the molds to confirm complete leaflet tissue formation, before harvesting. The formation process with a success rate of 90% could be clearly observed [Figure 2(C)]. If stronger materials were selected for the mold parts and if sterile conditions were more strictly controlled, a success rate of nearly 100% could be obtained. Furthermore, another advantage of the mold developed in this study was their prefabrication. Although the Biovalves had three projections, mimicking the sinus of Valsalva, the internal molds were easily removed and separated, due to the use of 3D digital printer-based molding.

The wall thicknesses of the conduit and leaflet parts of the Biovalves were almost the same (approximately 300 μm). However, the tensile strengths of the two parts were quite different. The tensile strength of conduit tissue was three times stronger than that of the leaflet, which was approximately equivalent to that of a natural goat leaflet. As the main component of both parts was collagen, we believe that the difference in the strength was depended on the density or orientation of the collagen fibers. The conduit part was formed around a rod. Thus, the collagen membrane formation process involved collagen fibers that may have pulled each other to completely cover the rod. This may have resulted in a higher density and better organization of the collagen fibers, leading to greater strength. On the other hand, the leaflet was formed in a small aperture between the sections of the mold. The collagen filled only the aperture, with little mechanical stimulation. This may have resulted in a lower strength of the tissue formed. In a separate study, we are developing a scanning haptic microscope that can observe the precise distribution of the elastic modulus on a cross-sectional surface of the tissue.[16,17] This is accomplished by segregating the elastin-rich and collagen-rich areas on the aortic tissue. Therefore, the differences in the density or the orientation of the collagen fibers, between the conduit and leaflet parts, will be obvious.

The leaflet thickness of human or goat aortic valves is about 200 μm, which is about 60% of that of the leaflets of the developed Biovalve. The thickness of the Biovalve leaflets depended on the thickness of the aperture in the molds for Biovalve preparation. In our preliminary examination for this study, in thin aperture less, tissue ingrowth was strongly inhibited. Therefore, to obtain thin leaflet as possible we selected the aperture thickness of 500 μm.

The encapsulating connective tissue was confirmed to be effective for use as leaflet tissue in heart valves in the first generation of Biovalve, developed in 2007.[11] The comparison of the several types of Biovalves is summarized in Table I. After repeated improvements, the type V pulmonary Biovalve was successfully used in a beagle dog model in 2010.[10]. However, the major disadvantage of that Biovalve was the structure of the leaflet mold, which resulted in considerable regurgitation. The three commissures between the leaflets had an aperture of approximately 1 mm. To avoid regurgitation, the apertures had to be sutured prior to implantation, which could potentially limit the Biovalve durability, particularly in systemic circulation. In the type VI Biovalve, the trileaflets were created in an open form, allowing the commissures to be connected without an aperture.[12] This resulted in a reduction in the regurgitation rate of 12.7%, while maintaining a high opening ratio of approximately 50%. The most recently improved Biovalve (Biovalve VII) involves a novel mold created using a 3D printer, yielding three projections that resemble the native sinuses of Valsalva in both shape and size. The vortex flow in the sinus of Valsalva plays an important role in the closure of the native semilunar valves and in the overall coronary flow. This version of the Biovalve showed excellent valvular function, with an extremely low regurgitation rate of <3%.

A fundamental requirement for the long-term performance of aortic heart valve leaflets is a dense, organized collagen matrix.[23] Based on the property of anisotropy, this matrix should, ideally, be developed prior to implantation. This study indicates that autologous *in vivo* tissue-engineered heart valves are promising aortic valve replacements, having minimal regurgitation in systemic circulation. Since Biovalves consist of a dense collagen matrix, valvular function was maintained for 10 days, even in saline. Moreover, the *in vivo* collagen matrix was retained despite unfavorable implantation conditions in the apico-aortic bypass method, in which the Biovalves were isolated from the native cardiovascular tissues by the interposition of artificial vascular grafts. In addition, the whole luminal surface was extremely smooth and well contoured, without any thrombus formations, despite the lack of endothelialization. These results indicate that the newly formed collagen in the Biovalves was robust and compatible with blood, suggesting that culturing, seeding, and conditioning autologous cells on a scaffold, as required for the creation of *in vitro* tissue-engineered valves, may be unnecessary. If Biovalves are used as anatomic aortic valve replacements, tissue ingrowth, including complete endothelialization, is expected. This would be similar to that demonstrated in the previous studies of pulmonary valve replacement with Biovalves[10] or the vascular implantation of Biotubes.[12,15]

CONCLUSION

3D printing was successfully demonstrated to be useful in the fabrication of the fine components required to create Biovalve molds. Biovalves, with sinuses of Valsalva, obtained from the mold satisfied the highly specialized systemic circulation requirements *in vitro* and *in vivo*. The Biovalve developed in this study is a conduit-type structure, which clinically needs an aortic root implant with reimplantation of the coronary ostia. We further aim to create a Biovalve

without a sinus of Valsalva conduit that is suitable for traditional aortic valve replace (AVR). We also aim to develop a Biovalve that is suitable for transcatheter AVR (TAVR), involving a valve leaflet construct that is connected/fixed to an expanding stent. In a previous study, metallic stents, covered with an autologous membranous tissues, were developed by applying this "in-body tissue architecture technology" to create Biocovered stents.[24] Using this method, Biovalves for use in both AVR and TAVR devices are under development.[25] We strongly believe that Biovalves have the potential to overcome the limitations of the currently used bioprosthetic valves, which are inherently prone to dysfunctional calcification and degeneration. This application may broaden future clinical opportunities for valve replacements. Biovalves do not require special handling techniques, either by the hospital staff or by the surgeon, thus facilitating their usage.

ACKNOWLEDGMENTS

The authors thank Ms. Manami Sone for her participation in this study.

REFERENCES

1. Le Tourneau T, Savoye C, McFadden EP, Grandmougin D, Carton HF, Hennequin JL, Dubar A, Fayad G, Waremboung H. Mid-term comparative follow-up after aortic valve replacement with Carpentier-Edwards and Pericarbon pericardial prostheses. Circulation 1999;100(19 Suppl):II11–II16.
2. Gandaglia A, Bagno A, Naso F, Spina M, Gerosa G. Cells, scaffolds and bioreactors for tissue-engineered heart valves: A journey from basic concepts to contemporary developmental innovations. Eur J Cardiothorac Surg 2011;39:523–531.
3. Berry JL, Steen JA, Koudy Williams J, Jordan JE, Atala A, Yoo JJ. Bioreactors for development of tissue engineered heart valves Ann Biomed Eng 2010;38:3272–3279.
4. Webb PA. A review of rapid prototyping (RP) techniques in the medical and biomedical sector. J Med Eng Technol 2000;24:149–153.
5. Curodeau A, Sachs E, Caldarise S. Design and fabrication of cast orthopedic implants with freeform surface textures from 3-D printed ceramic shell. J Biomed Mater Res 2000;53:525–535.
6. Gagg G, Ghassemieh E, Wiria FE. Effects of sintering temperature on morphology and mechanical characteristics of 3D printed porous titanium used as dental implant. Mater Sci Eng C Mater Biol Appl 2013;33:3858–3864.
7. Butscher A, Bohner M, Doebelin N, Hofmann S, Müller R. New depowdering-friendly designs for three-dimensional printing of calcium phosphate bone substitutes. Acta Biomater 2013;9:9149–9158.
8. Hockaday LA, Kang KH, Colangelo NW, Cheung PY, Duan B, Malone E, Wu J, Girardi LN, Bonassar LJ, Lipson H, Chu CC, Butcher JT. Rapid 3D printing of anatomically accurate and mechanically heterogeneous aortic valve hydrogel scaffolds. Biofabrication 2012;4:035005; doi:10.1088/1758-5082/4/3/035005.
9. Meseguer-Olmo L, Vicente-Ortega V, Alcaraz-Baños M, Calvo-Guirado JL, Vallet-Regi M, Arcos D, Baeza A. In-vivo behavior of Si-hydroxyapatite/polycaprolactone/DMB scaffolds fabricated by 3D printing. J Biomed Mater Res Part A 2013;101A:2038–2048.
10. Yamanami M, Yahata Y, Uechi M, Fujiwara M, Ishibashi-Ueda H, Kanda K, Watanabe T, Tajikawa T, Ohba K, Yaku H, Nakayama. Development of a completely autologous valved conduit with the sinus of Valsalva using in-body tissue architecture technology: A pilot study in pulmonary valve replacement in a beagle model. Circulation 2010;122(11 Suppl):S100–S106.
11. Hayashida K, Kanda K, Yaku H, Ando J, Nakayama Y. Development of an in vivo tissue-engineered, autologous heart valve (the biovalve): Preparation of a prototype model. J Thorac Cardiovasc Surg 2007;134:152–159.
12. Nakayama Y, Yahata Y, Yamanami M, Tajikawa T, Ohba K, Kanda K, Yaku H. A completely autologous valved conduit prepared in the open form of trileaflets (type VI biovalve): Mold design and valve function in vitro. J Biomed Mater Res B Appl Biomater 2011;99:135–141.
13. Nakayama Y, Ishibashi-Ueda H, Takamizawa K. *In vivo* tissue-engineered small-caliber arterial graft prosthesis consisting of autologous tissue (biotube). Cell Transplant 2004;13:439–449.
14. Gheorghe C, Iacob R, Bancila I. Olympus capsule endoscopy for small bowel examination. J Gastrointestin Liver Dis 2007;16:309–313.
15. Watanabe T, Kanda K, Yamanami M, Ishibashi-Ueda H, Yaku H, Nakayama Y. Long-term animal implantation study of biotube-autologous small-caliber vascular graft fabricated by in-body tissue architecture. J Biomed Mater Res B Appl Biomater 2011;98:120–126.
16. Moriwaki T, Oie T, Takamizawa K, Murayama Y, Fukuda T, Omata S, Kanda K, Nakayama Y. Variations in local elastic modulus along the length of the aorta as observed by use of a scanning haptic microscope (SHM). J Artif Organs 2011;14:276–283.
17. Oie T, Suzuki H, Murayama Y, Fukuda T, Omata S, Kanda K, Takamizawa K, Nakayama Y. Surface elasticity imaging of vascular tissues in a liquid environment by a scanning haptic microscope. J Artif Organs 2010;13:121–125.
18. Hayashida K, Kanda K, Oie T, Okamoto Y, Ishibashi-Ueda H, Onoyama M, Tajikawa T, Ohba K, Yaku H, Nakayama Y. Architecture of an in vivo-tissue engineered autologous conduit "Biovalve". J Biomed Mater Res B Appl Biomater 2008;86:1–8.
19. Nakayama Y, Yamanami M, Yahata Y, Tajikawa T, Ohba K, Watanabe T, Kanda K, Yaku H. Preparation of a completely autologous trileaflet valve-shaped construct by in-body tissue architecture technology. J Biomed Mater Res B Appl Biomater 2009;91:813–818.
20. Yamanami M, Yahata Y, Tajikawa T, Ohba K, Watanabe T, Kanda K, Yaku H, Nakayama Y. Preparation of in-vivo tissue-engineered valved conduit with the sinus of Valsalva (type IV biovalve). J Artif Organs 2010;13:106–112.
21. Takewa Y, Yamanami M, Kishimoto Y, Arakawa M, Kanda K, Matsui Y, Oie T, Ishibashi-Ueda H, Tajikawa T, Ohba K, Yaku H, Taenaka Y, Tatsumi E, Nakayama Y. In vivo evaluation of an in-body, tissue-engineered, completely autologous valved conduit (biovalve type VI) as an aortic valve in a goat model. J Artif Organs 2013;16:176–184.
22. Sumikura H, Nakayama Y, Ohnuma K, Takewa Y, Tatsumi E. In vitro evaluation of a novel autologous aortic valve (biovalve) with a pulsatile circulation circuit. Artif Organs 2014;38:282–289.
23. Mol A, Rutten MC, Driessen NJ, Bouten CV, Zünd G, Baaijens FP, Hoerstrup SP. Autologous human tissue-engineered heart valves: Prospects for systemic application Circulation 2006;114(1 Suppl):I152–I158.
24. Nakayama Y, Zhou YM, Ishibashi-Ueda H. Development of in vivo tissue-engineered autologous tissue-covered stents (biocovered stents). J Artif Organs 2007;10:171–176.
25. Mizuno T, Takewa Y, Sumikura H, Ohnuma K, Moriwaki T, Yamanami M, Oie T, Tatsumi E, Uechi M, Nakayama Y. Preparation of an autologous heart valve with a stent (stent-biovalve) using the stent eversion method. J Biomed Mater Res B Appl Biomater. Forthcoming.

Society For Biomaterials

Basic study of soft tissue augmentation by adipose-inductive biomaterial

Masaki Yazawa,[1] Taisuke Mori,[2] Yasuhide Nakayama,[3] Kazuo Kishi[1]

[1]Department of Plastic and Reconstructive Surgery, School of Medicine, Keio University, Tokyo, Japan
[2]Department of Pathology, National Cancer Center Laboratory, Tokyo, Japan
[3]Division of Medical Engineering and Materials, National Cerebral and Cardiovascular Center Research Institute, Osaka, Japan

Received 19 December 2013; revised 25 February 2014; accepted 12 April 2014
Published online 00 Month 2014 in Wiley Online Library (wileyonlinelibrary.com). DOI: 10.1002/jbm.b.33180

Abstract: Reconstructive surgery for tumor resection, trauma, and congenital anomaly involves volume augmentation with autologous tissue transfer. However, a healthy region is damaged as a donor site, and the autologous tissue is transferred like a patchwork to the recipient site. We have attempted to induce adipogenesis activity in artificial biomaterial that is injectable with an injection needle for soft tissue augmentation. First of all, the optimal dose of pioglitazone hydrochloride was examined with adipo-precursor cells in terms of the proliferator-activated receptor-γ mRNA expression levels affected by reagent *in vitro*. Then, salmon collagen with pioglitazone was adjusted in terms of the dose and the salmon collagen was injected into mouse back using an injection needle *in vivo*. At 4 weeks after implantation, the pioglitazone collagen gel was substituted by mature adipocytes in comparison with the case for control collagen gel without pioglitazone. These results are indicative of the possibility of promoting adipogenesis using collagen with pioglitazone as an adipose-inductive substance. © 2014 Wiley Periodicals, Inc. J Biomed Mater Res Part B: Appl Biomater 00B: 000–000, 2014.

Key Words: adipose, biomaterial, augmentation, soft tissue

How to cite this article: Yazawa M, Mori T, Nakayama Y, Kishi K. 2014. Basic study of soft tissue augmentation by adipose-inductive biomaterial. J Biomed Mater Res Part B 2014:00B:000–000.

INTRODUCTION

In recent years, advances in medicine have spectacularly improved the survival rate in tumor resection, trauma, and congenital anomaly. However, some patients cannot obtain a sufficient quality of life because of poor appearance after treatments. At present, reconstructive surgery for tumor resection, trauma, and congenital anomaly involves volume augmentation with autologous tissue transfer. However, a healthy region is damaged as a donor site, and the autologous tissue is transferred like a patchwork to the recipient site. Therefore, the quality of life of patients is not improved sufficiently.

Now, a new tissue transfer method without the problems at donor and recipient sites is required. We have attempted to induce adipogenesis activity in artificial biomaterial that is injectable using an injection needle, with the goal of its clinical application. To achieve this, pioglitazone hydrochloride was selected because it has been applied in clinical treatment as a diabetic medicine and has been reported to induce adipogenesis via peroxisome proliferator-activated receptor-γ (PPAR-γ).[1,2]

As an injectable artificial biomaterial, salmon collagen was selected because it is clinically available and should work as a scaffold for adipose tissue by ligand protein interaction.[3–7]

First of all, the optimal dose of pioglitazone was examined. Then, salmon collagen with pioglitazone was adjusted in terms of the dose and the salmon collagen was injected using an injection needle *in vivo*. Finally, adipogenesis at the recipient site was estimated in terms of the function of the artificial material as a transplant bed for adipogenesis.

MATERIALS AND METHODS

Animal care

The experimental procedure was authorized and reviewed by the Keio University Experimental Animal Center Committee (Approval no. 10256(0)).

Forty C3H/He/N mice (8 weeks, male, body weight 25–30 g; purchased from Charles River Laboratories Japan Inc., Tokyo, Japan) were used in the current study. All surgeries were performed in an animal-operating suite at the university.

Histological analysis

All tissue samples were obtained by mouse experiment and were fixed in 10% formalin and embedded in paraffin.

Correspondence to: M. Yazawa (e-mail: prsyazawa@gmail.com)
Contract grant sponsor: Japan Society for the Promotion of Science; contract grant number: KAKENHI 23792059

Subcutaneous transplanted materials were histologically evaluated.

Adipose precursor isolation and cell culture

To study adipo-precursor cells in terms of their PPAR-γ mRNA expression levels induced by the reagent *in vitro*, we isolated cells from the subcutaneous fat pad tissue of mice at a lower-back site. Briefly, tissue was minced and incubated for 1 h at 37°C in a rotary shaking bath at 100 rpm in digestion buffer containing collagenase (5 mg/mL) before being filtered through a 400-μm nylon mesh. The adipo-precursor cells were washed twice with serum-free Dulbecco's modified Eagle's medium (DMEM) (pH 7.4, 10 n*M* 4-(2-hydroxyethyl)-1-piperazineethanesulfonic acid (HEPES), containing penicillin/streptomycin) and incubated at 37°C under sterile tissue culture conditions. The adipo-precursor cells were expanded in bulk culture to avoid any biases resulting from cloning, and subjected to further analysis.

For cell proliferation assay, we used "passage two" adipose precursor cells as this would eliminate the hematocytes. About 1×10^5 cells were seeded into six cell culture plates in triplicate and counted at 14 days. For the induction of PPAR-γ mRNA expression, 100, 10, and 1 μ*M* pioglitazone (pioglitazone hydrochloride, Tokyo Chemical Industry, Tokyo, Japan), 200, 20, and 2 ng/mL insulin-like growth factor (IGF) 1 (PeproTech, NJ), and 200, 20, and 2 ng/mL IGF2 (PeproTech, NJ) were each added to the culture medium.

Quantitative reverse transcription PCR

Total RNAs were extracted with the RNeasy Mini kit (Qiagen, Valencia, CA) and reverse-transcribed using the SuperScript III RT-PCR system (Invitrogen, Carlsbad, CA) according to the manufacturer's protocol. We did not change the media for 2 weeks for the induction of adipocytes. One microliter of cDNA sample was amplified by PCR gene-specific primers. For quantitative RT-PCR (qRT-PCR), reactions were performed in triplicate using Fast Start Universal Probe Master (Roche Applied Science, Penzberg, Germany). The primer sets were as follows: for mouse PPAR-γ: 5′-ATCATCTACACGATGCTGGCC-3′ (forward), 5′-CTCCCTGGTCATGAATCCTTG-3′ (reverse); and for GAPDH: 5′-CACCATGGAGAAGGCCGGGG-3′ (forward), 5′-GACG GACACATTGGGGGTAG-3′ (reverse).

Statistical analysis

Data are expressed as mean ± SE (standard error). The relative mRNA expression levels were compared using unpaired *t*-test and all statistical analyses were performed using Statcel software (OSM, Japan). The results were judged significant at $p < 0.05$.

Adipogenesis by artificial biomaterial with pioglitazone *in vivo*

Nine C3H/He/N mice were used and maintained under specific pathogen-free conditions throughout this experiment. The optimal dose of pioglitazone was determined to be 10 μ*M* by previous cell proliferation assays. About 0.5% salmon collagen particles with and without pioglitazone (10 μ*M*) (0.9 g each, both from IHARA & Co., Ltd., Japan) were produced as follows. The salmon atelocollagen W/O (water in oil) emulsion was made by span20 (sorbitan monolaurate). The salmon collagen crosslinked by EDC (1-ethyl-3-(dimethylaminopropyl) carbodiimide hydrochloride) was settled down as particles to the water phase of 50% (vol/vol) EtOH. Dried particles were mixed with pioglitazone (10 μ*M*) solution and aspirated. The collagen particles with and without pioglitazone were dispersed in 0.9 mL of saline. About 0.1 mL of collagen gel with and without pioglitazone was injected under bilateral dorsal skin layer using an 18-G injection needle. The mice were then sacrificed and evaluated pathologically at 1, 2, and 4 weeks after operation. Three replicate samples were performed for each test. In addition, the area of adipose tissue was calculated in the histologic sections using software (Photoshop 7.0, Adobe, USA).

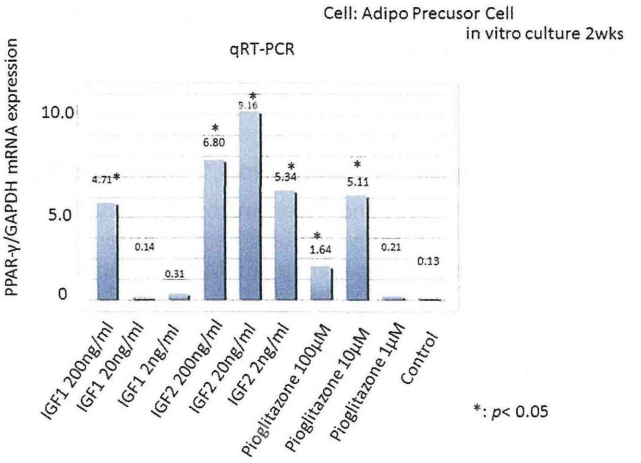

FIGURE 1. Pioglitazone and IGFs up-regulated PPAR-γ mRNA levels in mouse adipo-precursor cells. Mouse adipo-precursor cells were incubated for 2 weeks with pioglitazone, IGF1, or IGF2 at the indicated doses, and PPAR-γ mRNA levels were determined by qRT-PCR. *$p < 0.05$ versus control. [Color figure can be viewed in the online issue, which is available at wileyonlinelibrary.com.]

RESULT

Pioglitazone and IGFs up-regulated PPAR-γ mRNA levels

PPAR-γ is considered to be one of the master regulators of adipocyte differentiation (Figure 1).[8] To evaluate the potential effects of pioglitazone and IGFs on PPAR-γ expression, we exposed mouse adipo-precursor cells to these substances for 2 weeks and performed qRT-PCR. As shown in Figure 1, the dose responses of the expression level of PPAR-γ mRNA with pioglitazone, IGF1, IGF2, and control (without any reagent) were quantitatively analyzed in cultured cells. The PPAR-γ expression levels were efficiently up-regulated dose-dependently by all reagents, whereas 100 μ*M* pioglitazone caused cell toxicity (mean relative levels: pioglitazone 1 μ*M* vs. 10 μ*M* vs. 100 μ*M* = 0.21 vs. 5.11 vs. 1.64; mean relative levels: IGF1 2 ng/mL vs. 20 ng/mL vs. 200 ng/mL = 0.31 vs. 0.14 vs. 4.71; mean relative levels: IGF2 2 ng/mL vs. 20 ng/mL vs. 200 ng/mL = 5.34 vs. 9.16 vs. 6.80). The effective induction abilities of PPAR-γ by pioglitazone

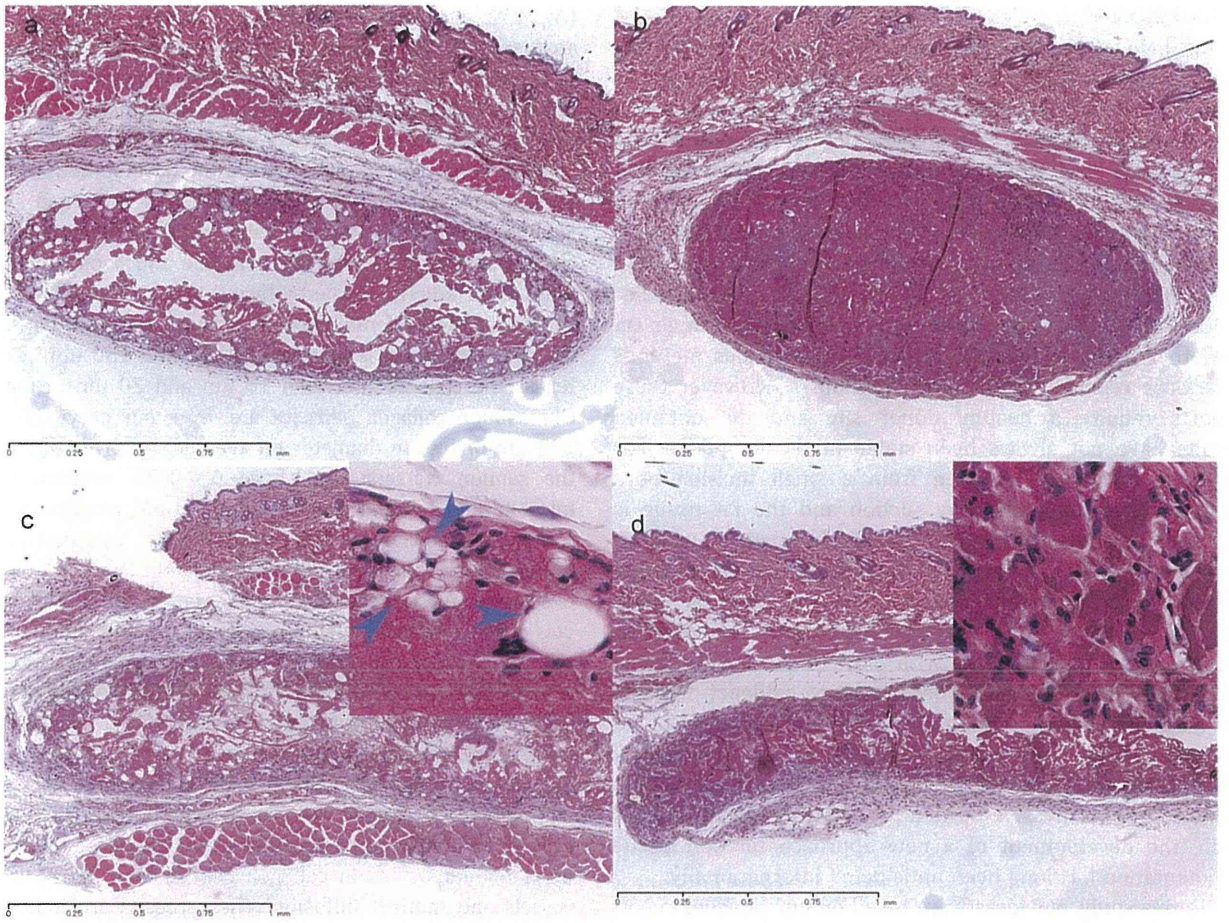

FIGURE 2. Photomicrographs of sections from implanted collagen gel after 1 week and 4 weeks. At 1 week after implantation, both the collagen gels were observed without any immune elimination (a, b). At 4 weeks after implantation, the pioglitazone collagen gel (c) was substituted by mature adipocytes (arrow heads) in comparison with the case for control gel (d). (a, c) Collagen gel with pioglitazone at 10 μM; (b, d) collagen gel only (H&E staining, original magnification 100× and insets 400×). [Color figure can be viewed in the online issue, which is available at wileyonlinelibrary.com.]

and IGFs were not significantly different from the control ($n = 3$; $p > 0.05$).

Quantification of induced adipose tissue *in vivo*

We evaluated the time course of the areas of adipose tissue induced by pioglitazone/collagen gel (induced group) that was comprised of mature adipose cells relative to the total implanted gel area (Figures 2 and 3). For mature adipose cells observed at the edge of the pioglitazone/collagen gel after one week of implantation, the average area percentage was 4.29%. In contrast, few adipose cells were observed in the collagen gels without pioglitazone (control group); the average area percentage was 0.343%. The collagen gels without pioglitazone as a control began to degrade without the induction of adipose cells from 2 weeks. In contrast, in the collagen gels with pioglitazone as an induced group, the replacement of adipose cells was observed. The induced group had higher proportions of adipose cells in the gels in a time-dependent manner after 2 weeks and 4 weeks. The average area percentages were 5.36% in the induced group and 0.394% in the control group after 2 weeks. They were 17.7% in the induced group and 1.20% in the control group after 4 weeks, as shown in Figure 3. There were statistically significant differences between the induced group and the control group ($p < 0.05$).

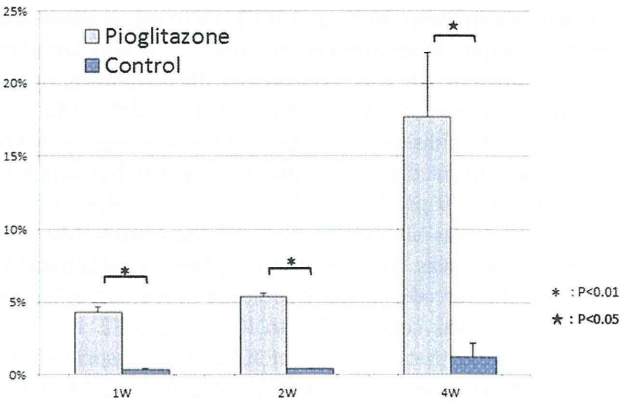

FIGURE 3. Area percentages of induced adipose tissue *in vivo*. [Color figure can be viewed in the online issue, which is available at wileyonlinelibrary.com.]

DISCUSSION

In the field of reconstructive surgery, operative techniques for autologous tissue transfer and medical technology in artificial materials have improved. To obtain autologous tissue, however, there is still a need for a donor site in a healthy body area, which is sutured to the recipient site like a patchwork for volume augmentation. This is not ideal in terms of patient satisfaction. In the case of hard tissue, artificial bone has already been developed into block and liquid types with processability for clinical applications, while liquid artificial bone is injectable with an injection syringe. On the other hand, in the case of soft tissue, various methods have been reported for fat augmentation.[9,10] However, these reports require a healthy donor site and the obtained results have not always been stable in the long-term. For example, fat tissue is taken from a small incision at a healthy area of a patient by suction and the fat tissue is injected into the recipient area of the patient using a syringe.[11] Besides, Kimura et al. reported a combination method involving autologous fat cells and artificial material.[12] The volume rate of grafted fat tissues is, nevertheless, unstable and unpredictable, with most of the volume being absorbed as time passes. These lines of evidence indicate the possibility of repetitive operations and overdose of fat grafting. These conventional methods for autologous fat grafting always need a healthy donor site and the patient is subjected to an invasive burden by repetitive operations. As such, the development of a new approach for soft tissue augmentation has long been anticipated internationally.

In this study, our ideas were based on our previous report that mesenchymal stromal cells induced adipocytes.[13] For an adjunct to artificial biomaterial, pioglitazone hydrochloride was focused on as a substance for adipose induction and maintenance.[14–16] Youm et al. reported that pioglitazone induces ectopic adipogenesis via PPAR-γ.[1] Pioglitazone hydrochloride is already used for diabetic patients in clinical applications.

Therefore, the optimal concentration of pioglitazone for the efficient induction and promotion of adipose tissue was examined. The mRNA levels of PPAR-γ, which is considered to be one of the master regulators of adipocyte differentiation,[17] were examined by qRT-PCR *in vitro*. IGF1 and IGF2 were used for comparison. The concentrations of each substance, pioglitazone, IGF1, and IGF2, were set at three levels using examples from previous reports.[18,19] It was found that 10 μ*M* pioglitazone was associated with a significantly high PPAR-γ mRNA level for adipo-precursor cells (Av. 5.11, $p < 0.05$). In addition, 100 μ*M* pioglitazone was associated with a significant difference from the control, but was lower than that for 10 μ*M* (Av. 1.64, $p < 0.05$). The effect of 1 μ*M* pioglitazone was almost the same as the control (Av. 0.21). About 10 μ*M* was thus set as the optimal concentration of pioglitazone for adipogenesis of adipo-precursor cells. Next, pioglitazone was compared with IGF1 and IGF2. It is interesting to note that all levels of IGF2 were associated with very high levels of PPAR-γ mRNA (2 μ*M*: Av. 5.34; 20 μ*M*: Av. 9.16; 200 μ*M*: Av. 6.80). In the examination of the effect of IGF1 on the PPAR-γ mRNA level, 200 μ*M* was the only level to show a significant difference from the control (Av. 4.71, $p < 0.05$). About 10 μ*M* pioglitazone was associated with similar PPAR-γ mRNA expression to IGF1 and IGF2, which are known to be PPAR-γ inducers. These results indicated that 10 μ*M* pioglitazone is reasonable as the optimal level for inducing PPAR-γ mRNA expression.

This study was intended to aid the development of clinical applications, so 10 μ*M* pioglitazone was examined *in vivo*. Salmon collagen, as an injectable artificial biomaterial, was chosen here as it is clinically available and should work as a scaffold for adipose tissue by ligand protein interaction.[3–7] We think that the preferable size of collagen particles for scaffold of cell proliferation is between 70 μm and 130 μm in diameter, as the cells are between 10 μm and 20 μm in diameter. Our salmon collagen particles are, from our previous results, 223 μm or less in diameter on average. In terms of adjusting the salmon collagen, we chose 0.3–0.5% solution for the injectable component and included 10 μ*M* pioglitazone. This conditioned collagen with or without pioglitazone was implanted into mouse back under the skin layer and observed over time. At 1 week after implantation, both the collagen gels were observed without any immune elimination. A small number of fat droplets were observed at the edge of the collagen gel with pioglitazone. At 4 weeks after implantation, the collagen gel with pioglitazone was substituted by mature adipocytes in comparison with the case for the collagen gel without pioglitazone. We think that the source of mature adipocytes in collagen gels is migrated mesenchymal stem cells or migrated adipo-precursor cells and that the nourishment for adipocytes in collagen gels is from both peripheral vessels and indirect diffusion. These results are indicative of the possibility of promoting adipogenesis by collagen supplemented with pioglitazone as an adipose-inductive substance.

In future, if larger volumetric adipogenesis becomes a reality, this result should be highly promising for the following factors:

1. Soft tissue augmentation after tumor resection;
2. Prevention of wound contracture and promotion of wound healing;
3. Prevention of perforation, scar formation, and stenosis of intestinal mucosa damaged by digestive endoscopy; and
4. Esthetic improvement of poor form caused by body surface asperity.

ACKNOWLEDGMENT

Authors thank Hatsumi Kobayashi and Masanobu Munekata (IHARA & Co., Ltd., Japan) for preparation of the salmon collagen with and without pioglitazone. The authors declare no conflicts of interest.

REFERENCES

1. Youm YH, Yang H, Amin R, Smith SR, Leff T, Dixit VD. Thiazolidinedione treatment and constitutive-PPARγ activation induces ectopic adipogenesis and promotes age-related thymic involution. Aging Cell 2010;9:478–489.
2. Schadinger SE, Bucher NLR, Schreiber BM, Farmer SR. PPARγ2 regulates lipogenesis and lipid accumulation in steatotic hepatocytes. Am J Physiol Endocrinol Metab 2005;288: 1195–1205.

3. Yunoki S, Nagai N, Suzuki T, Munekata M. Novel biomaterial from reinforced salmon collagen gel prepared by fibril formation and cross-linking. J Biosci Bioeng 2004;98:40–47.
4. Nagai N, Kubota R, Okahashi R, Munekata M. Blood compatibility evaluation of elastic gelatin gel from salmon collagen. J Biosci Bioeng 2008;106:412–415.
5. Nagai N, Nakayama Y, Zhou YM, Takamizawa K, Mori K, Munekata M. Development of salmon collagen vascular graft: Mechanical and biological properties and preliminary implantation study. J Biomed Mater Res B Appl Biomater 2008;87:432–439.
6. Nagai N, Nakayama Y, Nishi S, Munekata M. Development of novel covered stents using salmon collagen. J Artif Organs 2009; 12:61–66.
7. Kawaguchi Y, Kondo E, Kitamura N, Arakaki K, Tanaka Y, Munekata M, Nagai N, Yasuda K. In vivo effects of isolated implantation of salmon-derived crosslinked atelocollagen sponge into an osteochondral defect. J Mater Sci Mater Med 2011;22:397–404.
8. Rosen ED, Walkey CJ, Puigserver P, Spiegelman BM. Transcriptional regulation of adipogenesis. Genes Dev 2000;14:1293–1307.
9. Kelly JL, Findlay MW, Knight K, Penington A, Thompson EW, Messina A, Morrison WA. Contact with existing adipose tissue is inductive for adipogenesis in matrigel. Tissue Eng 2006;12:2041–2047.
10. Findley MW, Messina A, Thompson EW, Morrison WA. Long-term persistence of tissue-engineered adipose flaps on a murine model to 1 year: An update. Plast Reconstr Surg 2009;124:1077–1084.
11. Phulpin B, Gangloff P, Tran N, Bravetti P, Merlin JL, Dolivet G. Rehabilitation of irradiated head and neck tissue by autologous fat transplantation. Plast Reconstr Surg 2009;123:1187–1197.
12. Kimura Y, Ozeki M, Inamoto T, Tabata Y. Adipose tissue engineering based on human preadipocytes combined with gelatin microspheres containing basic fibroblast growth factor. Biomaterials 2003;24:2513–2521.
13. Allan EH, Ho PW, Umezawa A, Hata J, Makishima F, Gillespie MT, Martin TJ. Differentiation potential of a mouse bone marrow stromal cell line. J Cell Biochem 2003;90:158–169.
14. Kern PA, Marshall S, Eckel RH. Regulation of lipoprotein lipase in primary cultures of isolated human adipocytes. J Clin Invest 1985; 75:199–208.
15. Bodles AM, Banga A, Rasouli N, Ono F, Kern PA, Owens RJ. Pioglitazone increases secretion of high-molecular-weight adiponectin from adipocytes. Am J Physiol Endocrinol Metab 2006;291:E1100–E1105.
16. Yamanouchi K, Ban A, Shibata S, Hosoyama T, Murakami Y, Nishihara M. Both PPARγ and C/EBPα are sufficient to induce transdifferentiation of goat fetal myoblasts into adipocytes. J Reprod Dev 2007;53:563–572.
17. Gurnell M. Peroxisome proliferator-activated receptor gamma and the regulation of adipocyte function: Lessons from human genetic studies. Best Pract Res Clin Endocrinol Metab 2005;19:501–523.
18. Higashi Y, Holder K, Delafontaine P. Thiazolidinediones upregulate insulin-like growth factor-1 receptor via a peroxisome proliferator-activated receptor gamma-independent pathway. J Biol Chem 2010;285:36361–36368.
19. Kleiman A, Keats EC, Chan NG, Khan ZA. Elevated IGF2 prevents leptin induction and terminal adipocyte differentiation in hemangioma stem cells. Exp Mol Pathol 2013;94:126–136.

Superselective Shunt Occlusion for the Treatment of Cavernous Sinus Dural Arteriovenous Fistulae

Tetsu Satow, MD, PhD*
Kenichi Murao, MD, PhD‡
Toshinori Matsushige, MD*
Kenji Fukuda, MD*
Susumu Miyamoto, MD, PhD§
Koji Iihara, MD, PhD*

*Department of Neurosurgery, National Cerebral and Cardiovascular Center, Suita, Osaka, Japan; ‡Department of Neuroendovascular Therapy, Shiroyama Hospital, Habikino, Osaka, Japan; §Department of Neurosurgery, Kyoto University Graduate School of Medicine, Kyoto, Japan

Correspondence:
Tetsu Satow, MD, PhD,
Department of Neurosurgery,
National Cerebral and Cardiovascular Center,
5-7-1, Fujishirodai, Suita,
Osaka, 565-8565, Japan.
E-mail: tetsus@hsp.ncvc.go.jp

Received, May 7, 2012.
Accepted, February 5, 2013.
Published Online, March 27, 2013.

BACKGROUND: In treating cavernous sinus dural arteriovenous fistulae (CSdAVFs), transvenous embolization of the whole affected sinus is usually performed, which may result in the disturbance of normal venous drainage or permanent cranial nerve palsy.
OBJECTIVE: To describe superselective shunt occlusion of CSdAVFs.
METHODS: Between July 2005 and August 2011, we had 20 consecutive cases of CSdAVFs. In 14 cases (70%), we could detect the restricted locus of arteriovenous shunts by 3-dimensional rotational angiography and/or superselective arteriography. After navigating the microcatheter to the shunt segment, consecutive superselective arteriovenography was performed to confirm the location of the microcatheter at the proper position.
RESULTS: In 12 of 14 cases (85.7%) in which the shunt was restricted, coiling only in the small venous pouch or compartment, which was just downstream of the shunt point, led to complete disappearance of the shunt without obliterating the entire sinus. No recurrence or permanent cranial nerve palsy was observed during the follow-up period with a mean of 46 months (range, 3-69 months) in 12 cases treated by superselective shunt occlusion.
CONCLUSION: This technique, which enables complete extirpation of shunts by small amounts of coils, is a feasible way to treat CSdAVFs with excellent mid- to long-term results. Understanding of the angioarchitecture by 3-dimensional rotational angiography and consecutive superselective arteriovenography was useful. This method should be considered before sinus packing or mere obliteration of dangerous venous outlets.

KEY WORDS: Cavernous sinus, Dural arteriovenous fistula, Embolization, Transvenous

Neurosurgery 73[ONS Suppl 1]:ons100–ons105, 2013 DOI: 10.1227/NEU.0b013e31828ba578

Cavernous sinus dural arteriovenous fistulae (CSdAVFs) have been treated by a catheter-based approach, either transarterially, transvenously, or in combination. Among them, the transvenous approach was considered to be the most effective way to treat this disease.[1] In many cases, coil placement in the entire affected sinus has been performed.[2] This "entire sinus packing," however, carries the risk of disturbing the normal venous drainage through the cavernous sinus and the risk of permanent cranial nerve palsy (CNP) caused by the mass effect of the placed coils.[3-5]

ABBREVIATIONS: AVF, arteriovenous fistula; **CNP,** cranial nerve palsy; **CS,** cavernous sinus; **CSdAVF,** cavernous sinus dural arteriovenous fistula; **ECA,** external carotid artery; **3-D RA,** 3-dimensional rotational angiography; **SSSO,** superselective shunt occlusion

On the other hand, selective occlusion of the shunt segment (shunt point and small venous pouch or compartment downstream the shunt point) by detecting the shunt point can prevent the problems listed above, and a few case reports have noted this concept.[6-8] None of these reports, however, had documented the technical details of this treatment, and ultimately many coils were placed in the affected sinus.

Here we describe our experience in treating CSdAVFs by superselective shunt occlusion (SSSO), with a focus on its concept as well as technical tips.

METHODS

Patients and Methods

Our study is based on 20 consecutive patients with CSdAVFs treated at our institution between July 2005 and August 2011.

The diagnosis was made on transfemoral 6-vessel angiography including bilateral internal carotid arteries, external carotid arteries (ECAs), and vertebral arteries. Injections from the bilateral common carotid arteries were also performed so as not to miss the involvement of ascending pharyngeal arteries.[9] Three-dimensional rotational angiography (3-D RA) was routinely performed in later cases to assess the whole angioarchitecture and to not miss any involved vasculature.

Technical Aspects of SSSO

At the time of intervention, which was done with the patient under general anesthesia to eliminate motion artifacts, diagnostic angiography was performed again of the ECA, and accurate information was obtained regarding which branch of the ECA was involved. Also, a 6-French guiding catheter was navigated to the ipsilateral internal jugular vein through the femoral vein, in which a 4-French catheter was introduced coaxially.

After detection of the involved branches, a microcatheter was placed in 1 of the involved branches of the ECA, where superselective arteriography was performed to confirm the shunt segment.

The next step was performed on the venous side. Another microcatheter was introduced into the affected cavernous sinus (CS) via the inferior petrosal sinus, which was approached by the 4-French catheter regardless of its patency.[10,11] In the affected CS, this venous-sided microcatheter was advanced to the major venous outlets (eg, the superior ophthalmic vein, sphenoparietal sinu, and superior petrosal sinus) to understand the structure of the affected sinus before reaching the shunt segment and to secure accessibility of the major outlet even if SSSO failed to eliminate shunt flow.

On reaching the shunt segment, contrast was injected from the microcatheter in the feeding artery, followed by a contrast injection from the venous-sided microcatheter for superimposition. This maneuver, which we named "consecutive superselective arteriovenography," was performed to confirm that the microcatheter on the venous side was located in the shunt segment.

Finally, the shunt segment was obliterated with soft, electrically detachable coils.

RESULTS

The characteristics of the cases in this series are summarized in Table 1. Among the 20 patients in this study, 15 were women, and the mean age was 67.5 years old. Initial symptoms were ocular (chemosis and/or exophthalmos) in 13 patients and CNP in 11. The location of the shunt was clearly identified in 14 patients, and the shunt point was located outside the CS in 7.

In all patients, the shunt was diminished by transvenous coil placement, and SSSO was defined as a coil mass not exceeding more than 1 compartment of the CS.

SSSO was achieved in 12 of 14 cases (85.7%) with shunts restricted to the small compartment. In 2 patients, SSSO was attempted but failed; dislocation of the microcatheter out of the shunt segment before placement of sufficient coils for obliteration occurred in 1 patient (patient 7), and navigation of the microcatheter to 1 of the 2 shunt segments failed in the other (patient 18).

TABLE 1. Profiles and Characteristics of the Cases in This Study[a]

Patient	Age, y	Sex	Side	Barrow Type	Initial Symptoms	Shunt Location	SSSO	Worsening of Symptoms Post IVR	Persistent or Newly Developed Symptoms	Duration, d	FU, mo
1	62	F	R	D	C, VI	AI[b]	Yes	Yes	VI	7	59
2	50	F	L	C	C, E	PS	Yes	No	None		69
3	75	F	R	D	C, VI	AI[b]	Yes	No	None		60
4	76	F	R	C	C, E, VI	AI[b]	Yes	No	None		65
5	58	M	L	D	C, E, VI	AI[b]	Yes	No	None		59
6	73	F	R	D	C, E	Diffuse	No	Yes	C	8	54
7	22	F	L	D	V	AI	No	Yes	VI	1	52
8	68	M	R	D	C, E, VI	Diffuse	No	Yes	III, VI	Permanent	52
9	64	F	R	D	C, E	PS[c]	Yes	Yes	VI	2	52
10	67	M	R	D	VI	PS	Yes	Yes	VI	30	44
11	74	F	L	D	E	PS	Yes	No	None		36
12	76	F	B	D	C, E	Diffuse	No	Yes	VI	90	24
13	70	F	R	D	C, VI	PS	Yes	No	None		33
14	83	F	L	D	C, VI	PS	Yes	No	None		24
15	42	F	R	D	V	Diffuse	No	Yes	III, VI	Permanent	24
16	63	F	R	D	None	Diffuse	No	No	None		20
17	63	F	L	D	C, VI	Diffuse	No	No	None		18
18	53	M	R	D	VI	PS, M	No	Yes	III, VI	7	12
19	71	M	L	C	VI	PS[c]	Yes	No	None		6
20	76	F	R	B	C, E	M[b]	Yes	No	None		6

[a]SSSO, superselective shunt occlusion; IVR, interventional radiology; FU, follow-up; R, right; C, chemosis; VI, abducens palsy; AI, anteroinferior compartment; L, left; E, exophthalmos; III, oculomotor palsy; V, trigeminal dysesthesia in V1 lesion; M, medial compartment; PS, posterosuperior compartment.
[b]Shunt located in paracavernous region.
[c]Two distinct shunts located in paracavernous region.

Entire sinus packing was performed instead to eliminate the shunt in these 2 patients, in the same way as the remaining 6 patients with diffuse shunts.

Clinical follow-up was performed in all patients (mean length of follow-up, 40 months [range, 6-69 months]). All patients were examined by an ophthalmologist before and after the procedure. During the follow-up period, referral to the ophthalmologist was performed whenever the patient reported visual symptoms or the external ocular movement of the patient looked abnormal.

In patients treated by SSSO, whose mean follow-up period was 48 months, transient abducens nerve palsy occurred in 3 of 12 patients (25%) which was resolved within 1 month, whereas permanent CNP occurred in 2 patients (25%) with sinus packing.

Radiological follow-up was done by conventional angiography at 3 to 6 months after the procedure in 11 patients and by magnetic resonance angiography in all patients annually, and no recurrence was detected in patients with SSSO. In 2 patients with sinus packing, however, recurrence of the shunts were detected, and additional coils were placed.

ILLUSTRATIVE CASES

Patient 5

This 76-year-old woman presented with right chemosis and abducens palsy. Cerebral angiography revealed a Barrow type D CSdAVF (Figures 1A and 1B). At the time of the procedure, a microcatheter was advanced into the shunt segment via the transvenous approach. After the location of the microcatheter was confirmed by consecutive superselective arteriovenography (Figures 1C and 1D), the shunt segment was obliterated with

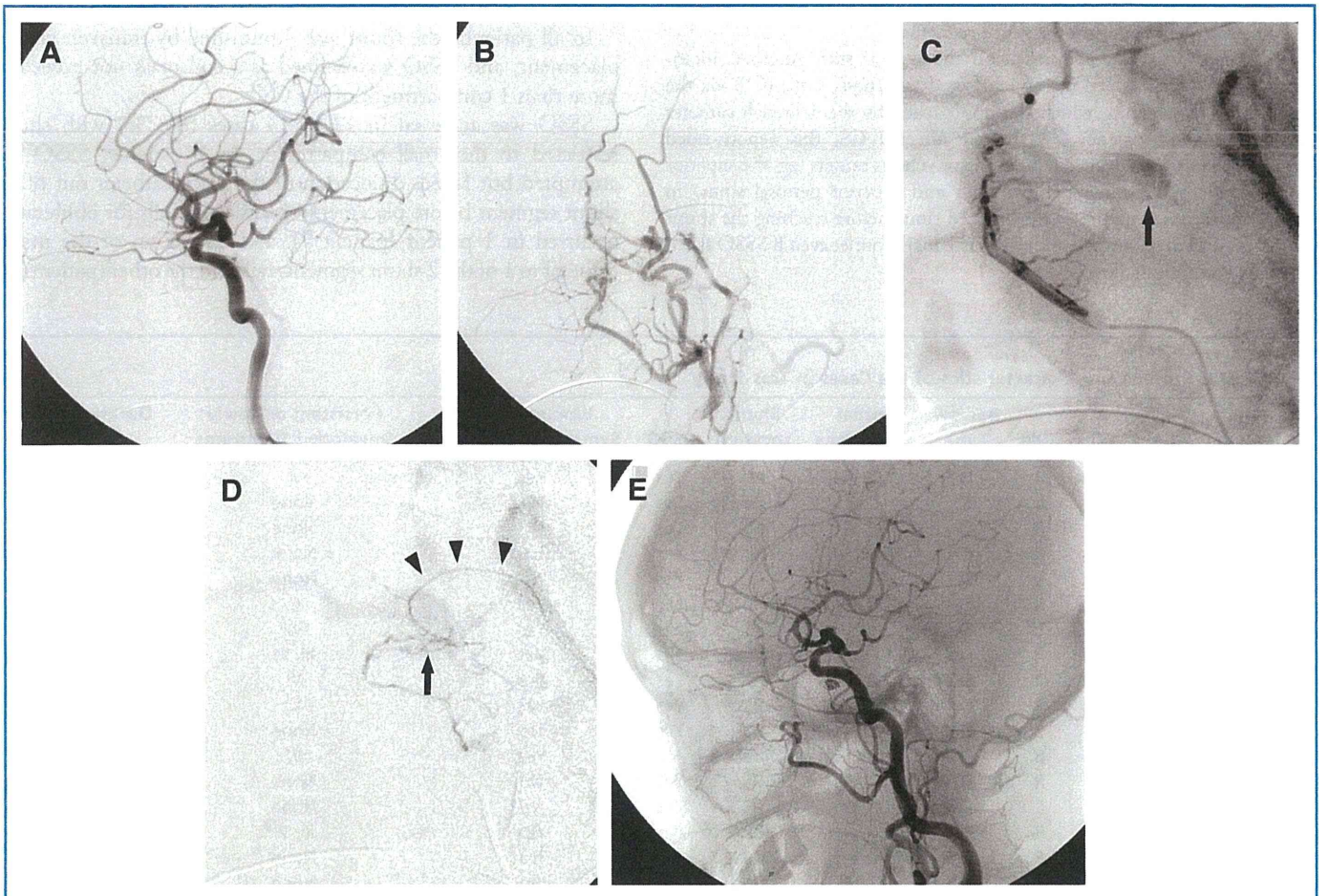

FIGURE 1. *Patient 5. Branches of both the right internal carotid artery (ICA) (lateral view) (A) and external carotid artery (ECA) (lateral view) (B) were involved and diagnosed as a Barrow type D cavernous sinus dural arteriovenous fistula. The middle meningeal artery (MMA) and the artery of foramen rotundum were the feeding arteries from right ECA. During the procedure, a microcatheter was located in right MMA and another microcatheter was in the paracavernous vein. The shunt and cavernous sinus were visualized by arterial injection (C), followed by venous injection (D) to confirm the tip of the venous-sided microcatheter in the shunt segment. The tip of the venous-sided microcatheter is indicated by an arrow, and the course of the microcatheter is indicated by arrowheads. The shunt segment was obliterated with 5 bare platinum coils. Postprocedural angiograms of the right common carotid artery (lateral view) (E) showed the extirpation of the shunt. Note the small size of the coil mass that was located inferior to the right ICA.*